

A new mid-infrared map of the BN/KL region using the Keck telescope

R. Y. Shuping¹ & Mark Morris²
Div. of Astronomy & Astrophysics, UCLA
MS 8371, Los Angeles, CA 90095-1562

and

John Bally³
Center for Astrophysics & Space Astronomy, University of Colorado
Campus Box 389, Boulder, CO 80309-0389

ABSTRACT

We present a new mid-infrared ($12.5\ \mu\text{m}$) map of the BN/KL high-mass star-forming complex in Orion using the LWS instrument at Keck I. Despite poor weather we achieved nearly diffraction-limited images ($\text{FWHM} = 0.38''$) over a roughly $25'' \times 25''$ region centered on IRC2 down to a flux limit of ≈ 250 mJy. Many of the known infrared (IR) sources in the region break up into smaller sub-components. We have also detected 6 new mid-IR sources. Nearly all of the sources are resolved in our mosaic. The near-IR source “n” is slightly elongated in the mid-IR along a NW–SE axis and perfectly bisects the double-peaked radio source “L”. Source n has been identified as a candidate for powering the large IR luminosity of the BN/KL region ($L = 10^5\ L_\odot$). We postulate that the $12\ \mu\text{m}$ emission arises in a circumstellar disk surrounding source n. The morphology of the mid-IR emission and the Orion “hot core” (as seen in NH_3 emission), along with the location of water and OH masers, is very suggestive of a bipolar cavity centered on source n and aligned with the rotation axis of the hypothetical circumstellar disk. IRC2, once thought to be the dominant energy source for the BN/KL region, clearly breaks into 4 sub-sources in our mosaic, as seen previously at $3.8 - 5.0\ \mu\text{m}$. The anti-correlation of mid-IR emission and NH_3 emission from the nearby hot core indicates that the IRC2 sources are roughly coincident (or behind) the dense hot core. The nature of IRC2 is not clear: neither self-luminous sources (embedded protostars) nor external heating by source I can be definitively ruled out. We also report the discovery of a new arc-like feature SW of the BN object, and some curious morphology surrounding near-IR source “t”.

Subject headings: Stars: formation — stars: early-type — ISM: outflows — ISM: individual (BN/KL, OMC 1) — infrared: ISM

1. Introduction

Because of its proximity (450 pc, Genzel & Stutzki 1989), the OMC 1 region, which includes the Becklin-Neugebauer object and the Kleinmann-Low nebula (BN/KL) and the Orion

“hot core”, is among the most studied regions of high-mass star formation in the sky. An outstanding uncertainty about this region is the source of the $\sim 10^5\ L_\odot$ of infrared (IR) luminosity from BN/KL. Though many individual peaks of thermal infrared (7 to $24\ \mu\text{m}$) emission have been identified (Lonsdale et al. 1982), many may not be self-luminous. The VLA studies by Menten & Reid (1995) indicate that, in addition to the BN object, the region contains at least two additional

¹shuping@astro.ucla.edu

²morris@astro.ucla.edu

³John.Bally@colorado.edu

ultra-compact radio sources, I and L, separated by about $3''$ from each other (1,500 AU in projection). Radio source L is coincident with IR source “n” (Lonsdale et al. 1982). Recent mid-IR studies of the region suggest that the hot stars powering these compact H II regions may be sufficient to drive the enormous IR flux from BN/KL (Gezari et al. 1998).

The Orion “hot core” is a warm, dense cloud ($T > 220$ K, $n(\text{H}_2) = 5 \times 10^7 \text{ cm}^{-3}$) in the SE region of BN/KL, first observed in ammonia emission (Morris et al. 1980). An unusually high number of hydrogen-saturated molecules are observed toward the hot core, perhaps due to the evaporation of icy grain mantles (Blake et al. 1987; Brown et al. 1988). The velocity centroid of the “shell masers” masers surrounding radio source I is nearly identical to the LSR velocity of the hot core ($v_{\text{lsr}} = 5 \text{ km s}^{-1}$), which suggests that the two are physically related. The *absence* of any IR emission and the morphology of the ammonia emission in the vicinity also suggests that radio source I is embedded in the hot core (Gezari et al. 1998; Wilson et al. 2000). Hence source I is probably responsible for most of the heating and chemistry in the hot core.

Sources I and n are both associated with strong OH, H_2O , and SiO maser emission (Johnston et al. 1989; Genzel et al. 1981). An expanding arcminute-scale complex of high velocity ($v = 30$ to 100 km s^{-1}) H_2O masers surrounds the entire OMC 1 region, with a center of expansion that coincides, within several arcseconds, with source n (Genzel et al. 1981; Menten & Reid 1995). In addition to this high-velocity flow, a low-velocity arcminute-scale cluster of much brighter maser spots is associated with this expansion ($v_{\text{expansion}} = 18 \pm 2 \text{ km s}^{-1}$). As shown by Gaume et al. (1998), the so-called 22-GHz H_2O “shell” masers, which were mostly resolved-out in the VLBI observations of Genzel et al. (1981), are concentrated in a $2''$ by $0.5''$ strip centered on source I and are oriented roughly orthogonal to the bipolar CO outflow emerging from OMC 1 (Chernin & Wright 1996). Bright SiO maser emission lies within $0.1''$ of source I, and consists of four clusters of maser spots having velocities very similar to those of the H_2O shell masers. Greenhill et al. (1998) and Doeleman et al. (1999) found that these masers are concentrated into four

linear chains located north, east, south, and west of source I. Contrary to prior conclusions, a new analysis by Greenhill et al. (2003) suggests that these masers trace a disk seen roughly edge-on with a projected rotation axis at $\text{PA} \sim 45^\circ$ and a bipolar wind impacting the surrounding dense medium.

Radio CO line emission indicates that there is also a fast (30 to 100 km s^{-1}), weakly collimated bipolar outflow emerging from the OMC 1 region with a blue-shifted lobe toward the northwest. The OMC 1 outflow has a mass of about $10 M_\odot$ and a kinetic energy of about 4×10^{47} ergs (Kwan & Scoville 1976). There are also “fingers” of H_2 emission, presumably from shocked gas, pointing away from the BN/KL region to the NW and SE. The OMC 1 outflow and the H_2 fingers (Allen & Burton 1993; Stolovy et al. 1998; Schultz et al. 1999; Kaifu et al. 2000) appear to indicate that a powerful ejection occurred in OMC 1 relatively recently. The H_2 finger system consists of over a hundred individual bow shocks which delineate a relatively wide-angle bipolar outflow toward $\text{PA} \approx 315^\circ$ with an opening angle of more than 1 radian in each lobe. The proper motion vector field of the H_2 line-emitting knots, as observed using *Hubble Space Telescope* (HST), has been interpreted as an explosion that occurred about 1010 ± 140 years ago (Lee & Burton 2000; Doi et al. 2002). This is consistent with the OMC 1 outflow observed in CO.

In this paper we present the highest spatial resolution map at $12.5 \text{ } \mu\text{m}$ of the BN/KL region to date.¹ In the next section we describe our observations using the LWS instrument on Keck I and the data analysis applied to produce the mosaic. In Section 3 we present our results, including 6 new mid-IR sources, and new morphologies for IRc2 and IR source n. In Section 4 we discuss the interpretation of some of our results, especially for sources n, I, and IRc2. We also try to rationalize the various outflows in the region and some curious features surrounding near-IR source “t”. Summary and conclusions are given in Section 5.

¹Note added during review: Another dataset obtained with LWS on the Keck I telescope has just been published by Greenhill et al. (2004) and covers some of the same fields in BN/KL as presented here.

2. Observations & Data Analysis

Observations of the BN/KL region were made using the Keck Observatory facility mid-IR camera LWS on UT 16 November 2002. LWS is a mid-IR imaging and spectroscopy instrument mounted on the forward Cassegrain focus of Keck I, employing a Boeing 128×128 As:Si BIB array with a $10.2 \times 10.2''$ field of view (Jones & Puetter 1993). Weather conditions were poor on UT 16 November 2002: the thermal background and atmospheric transmission varied by $\sim 50\%$ throughout the first half of the night. Approximately 30 individual observations (frames) were made of the BN/KL region at slightly overlapping positions using the $12.5\mu\text{m}$ filter ($12 - 13 \mu\text{m}$ bandpass with $> 80\%$ transmission). The chopping secondary mirror was driven at 2 Hz with a $30''$ E–W throw. Each frame was observed using the standard mid-IR chop-nod technique with two chopping positions “+” (on-source) and “-” (off-source); after chopping with the source in chop-beam “+”, the telescope was nodded along the chop axis so that the object would sit in chop-beam “-”, and chopping would continue. Each frame was observed for one complete chop-nod cycle, yielding a total on-source integration time of 27.6 seconds per mosaic frame. The standard stars β Peg, β And, and β Gem were also observed throughout the night for PSF determination and flux calibration. Our data are nearly diffraction limited at $12.5 \mu\text{m}$ with PSF FWHM = $0.38''$ and a Strehl ratio of 35%.

The LWS instrument saves all coadded data in individual chop and nod beams for each observation frame. The data were reduced by first finding and eliminating bad pixels in the raw data and then differencing the chop beams for each nod position. There were very few contaminating sources in our off-source chop beams: in these cases we merely threw out the offending chop pair and used the chop pair from the other nod position. Typically there was some residual sky signal left over after differencing. In order to create a smooth mosaic, we opted to eliminate this residual by calculating a sky mode and subtracting the value from the differenced images. While this effectively reduces the background to near zero, it also eliminates any diffuse nebular emission from the region. A gain map for the detector was created using an average of the off-source chop positions

for each chop-nod cycle, correcting for the dark current which we measured at the start of the night. This gainmap was then divided into the differenced chop-beam data. We found that, after nodding, the telescope did not always return the target to the exact same position on the detector, so we registered the nod position data using the cross-correlation of the two images and then coadded to create a final image for each telescope pointing. Reduced images for each pointing were then combined into a mosaic by registering on sources common to successive frames. The final mosaic is shown in Figure 1. Because of our frame overlapping strategy, we inadvertently missed one small region of BN/KL inbetween IRc2 and BN (shown as a dashed box in Figure 1).

A linear astrometrical solution for the completed mosaic was determined using the coordinates for BN (Menten & Reid 1995) and IRc7 (Gezari et al. 1998). The plate scale was determined to be $0.0805'' \text{ pixel}^{-1}$. Astrometrical errors were determined from the positional errors for BN and IRc7 (Gezari et al. 1998), the centroiding accuracy (< 0.5 pixel), and the offset from IRc7 or BN (whichever is closer). Positional errors range from $0.1''$ near IRc7 and BN to $0.3''$ at the edge of the mosaic. No attempt has been made to measure or correct for optical distortion, which is assumed to be small over the (very narrow) field of view.

Due to highly variable atmospheric transmission, flux calibration using the observed standards was not reliable. Instead we calibrated the entire mosaic using known fluxes for BN and IRc2 from (Gezari et al. 1998). Since the instrumental response varied from frame to frame in the mosaic, the flux calibration for any frame that does not contain BN or IRc2 can deviate significantly from those frames that do. The regions around IRc2, IRc7, and BN were observed multiple times, allowing us to determine a maximum variation (2σ) in the flux solution from frame to frame of $\sim 25\%$. The uncertainty in the known fluxes of BN and IRc2 at $12 \mu\text{m}$ is roughly 10% (Gezari et al. 1998), so the absolute flux calibration error ($\approx 2\sigma$) for our mosaic ranges between 10 and $\sim 27\%$. The 3σ flux limit for our data is approximately 250 mJy for a compact source measured in a 15-pixel-radius aperture.

3. Results

The 12.5 μm mosaic of BN/KL presented here is the highest spatial resolution mid-IR map of the region to date. Even at this resolution (PSF FWHM = 0.38") all the detected sources are resolved – there are no point sources down to our flux limit. Many known IR sources do break up into multiple compact sources, but even these sub-components are resolved. We have also detected 6 new mid-IR sources, one near BN which we have called the “southwest arc”, and 5 more which we have named IRc18 through 22, following Gezari et al. (1998). Positions for each of the sources relative to BN are given in Table 1. The uncertainty in the relative position is dominated by the offset from IRc7 or BN, as discussed in Section 2, and ranges from 0.1" to 0.3". We have also measured the flux for a handful of the most compact sources, using a large circular aperture and an outer annulus to determine the background flux density and its variance (Table 1). The flux uncertainty is dominated by variations caused by poor weather conditions (Section 2) but is not larger than $\approx 27\%$.

The mid-IR emission from the BN/KL region is generally thought to fall into two categories: Relatively dense clouds heated by external UV radiation from local high-mass stars embedded in the region, and dense regions heated by embedded YSOs. Most of the mid-IR sources (except for BN and n) are not seen at wavelengths less than a few microns owing to the significant (but patchy) foreground extinction associated with OMC 1. IRc3, 4, 5, and 6 have relatively cool mid-IR colors and polarizations consistent with external illumination (Gezari et al. 1998; Dougados et al. 1993; Minchin et al. 1991), most likely from sources I and n. In our data, IRc3 and 6 break up into smaller fragments, but there is no evidence of point sources which might be interpreted as embedded young stars. BN, source n, and IRc2, 7, 11, and 12 all have compact quasi-elliptical morphologies suggestive of dense clumps with embedded YSOs. In addition, these sources have much warmer mid-IR colors indicative of embedded objects (though the clumps would also be heated by external UV radiation) (Gezari et al. 1998).

The structure of IRc2 at 12 μm is similar to that seen at 4 – 5 μm , but not identical (Figure 2). Four

unresolved sources (A – D) have been detected at L' – with marginally resolved counterparts at 4.0 and 5.0 μm (Dougados et al. 1993). The morphology of IRc2 is clearly wavelength dependent from 3.8 to 12.5 μm : the eastern peak of IRc2 at 12.5 μm lies between A and B; and the peak of 12.5 μm emission near source C is offset from that source by about 0.5" to the SE. The faint emission just north of source D, first identified as a “jet-like” feature by Dougados et al. (1993), shows up as a distinct compact source at 12.5 μm which we have named “E” (Figure 3). Note that none of these IRc2 sources have been detected at 2 μm (e.g., Lonsdale et al. 1982; Schultz et al. 1999). Though very close (within 0.5"), source A is not coincident with source I. The nature of IRc2 and radio source I will be discussed in Section 4.

IR source n coincides with the double radio continuum source “L” (N and S), which has been identified as a possible source of significant ionizing radiation in the BN/KL region (Menten & Reid 1995). Source n appears as an unresolved point source throughout the near-IR (Lonsdale et al. 1982; Dougados et al. 1993). At 12 μm , however, source n appears elongated along a NW-SE position angle (Figure 3), perfectly bisecting the northern and southern components of radio source L (Figure 1) – suggestive of a circumstellar disk straddled by ionized bipolar cavities (or lobes, see Section 4). The uncertainty in the 12 μm position of source n (0.1") is smaller than the $\sim 0.2''$ separation between n and both components of L.

Though limited to one bandpass, the increased sensitivity of our dataset over previous efforts has revealed some new mid-IR sources in the BN/KL region: IRc18 – 22 (following Gezari et al. (1998)) and the “BN SW Arc”. The concentric relationship to BN suggests that the SW Arc is a nearby shell of heated gas and dust. Due to the inhomogeneous nature of the BN/KL region and the lack of data at other wavelengths, we can only speculate on the nature of the SW arc: it may be externally heated by UV radiation or is possibly a portion of a shocked, compressed shell created by an outflow or jet from BN. Source IRc18 is compact but still resolved, and may have a counterpart at 4 μm (Dougados et al. 1993). IRc19 is an irregularly shaped source just southwest of IR source “q” (Lonsdale et al. 1982); it is not clear whether the two are related. Source IRc20 appears as a

“bridge” between IRc7 and 3. This feature is also seen clearly at $4\ \mu\text{m}$ (Dougados et al. 1993). IRc21 is just north of IRc2 and may be associated with a bright knot of H_2 emission immediately to the west (see Figure 4). IRc22 appears to be associated with IR source “t” (Lonsdale et al. 1982) and will be discussed further below.

4. Discussion

4.1. IR Source n

There is a significant anticorrelation between the $12.5\ \mu\text{m}$ emission in our map and NH_3 emission from the “hot core” (Figure 5), suggesting that most of the mid-IR sources are *at the same distance or behind* the hot core. The very dark regions in our mid-IR mosaic – the roughly triangular region NW of n and the larger region SE of n – coincide very nicely with the NH_3 emission peaks (the correlation is most dramatic in the $6.79\ \text{km s}^{-1}$ channel of NH_3). Source n sits precisely at the waist of this emission. The mid-IR and NH_3 contours immediately surrounding source n are highly suggestive of bipolar cavities, with opening angles of $\sim 90^\circ$, aligned nearly perpendicular to the long axis of source n. In addition, most of the OH and H_2O masers in the entire BN/KL region can be found within an extension of the conical regions defined by these cavities (Figure 5) suggesting that these regions have been cleared by an outflow(s) from source n and that this outflow(s) is responsible for the masers.

The bipolar cavity defined by the mid-IR, NH_3 , and maser emission, along with the elongated structure of n at $12\ \mu\text{m}$, strongly suggests that n has a circumstellar disk with a rotation axis oriented NE–SW. The unresolved near-IR flux from n would be from the stellar photosphere and/or hot inner portion of the disk. The $12\ \mu\text{m}$ emission presumably arises in the outer portions of the disk (at hundreds of AU), where temperatures are a few hundred Kelvin, and hence could be resolved in our data. The FWHM at $12\ \mu\text{m}$ along source n’s long axis ($\text{PA} = 131^\circ$) is $0.57''$. Source n is unresolved along the short axis of mid-IR emission. If we assume a distance of 450 pc to OMC 1, source n must be 255 AU in diameter and < 167 AU in projected height, leading to a disk inclination of $> 50^\circ$. The disk cannot be edge-on, however, or source n would not be detected

at near-IR wavelengths owing to extinction of the stellar photosphere and inner disk by the outer, flared regions. The polarization angle and linear fraction for source n at $3.8\ \mu\text{m}$ (Minchin et al. 1991; Dougados et al. 1993) is consistent with this disk interpretation. The elongated radio source L, bisected perfectly by the mid-IR disk, may be emission from an ultra-compact bi-polar H II region above and below the disk or perhaps a jet and counter-jet. The rotation axis of the disk would be along $\text{PA} \approx 41^\circ$, in near perfect alignment with source L (N and S) and the bipolar cavities to the NE and SW. Because of its significant radio continuum emission, source n has already been identified as a possible contributor to the energetics of the BN/KL region (Menten & Reid 1995). Our data, coupled with the NH_3 observations of the hot core and the maser spots observed throughout BN/KL, suggest a disk and outflow morphology, as would be expected for a young, high-mass star.

4.2. Source I and IRc2

The strong radio continuum from source I, indicative of an ultra-compact H II region, suggests that it also is a significant energy source for the BN/KL region (Menten & Reid 1995). Source I has not been detected in the IR, however, indicating that if it is indeed a hot, young star, it must be obscured by over 60 visual magnitudes of dust, placing it within or on the far side of the hot-core (Gezari et al. 1998). Observations of the 86 GHz SiO masers led to an interpretation, at first, of an outflow from source I aligned with $\text{PA} \sim -45^\circ$ (Greenhill et al. 1998). New VLBA observations, however, suggest that the SiO masers arise in a disk seen nearly edge-on with a rotation axis at $\text{PA} \sim 45^\circ$ (Greenhill et al. 2003). In this picture, the water masers centered on source I (the “shell” masers) are due to a wide angle bipolar outflow from I impacting the surrounding dense natal material (Greenhill et al. 2003). Indeed, the shell masers trace very closely the NH_3 contours surrounding source I and the mid-IR contours in our mosaic (Figure 6), suggesting that they arise in the walls of a cavity excavated out of the hot core gas by bipolar outflows from source I (Wilson et al. 2000).

The nature of the IRc2 sources (A – E) is not entirely clear. Because of their proximity to source I on the sky and the fact that the mid-IR emis-

sion comes from a location which is at or behind the hot core (in which source I is most likely embedded), it seems that the IRc2 sources are associated with source I. The silicate extinction factor ($9.8 \mu\text{m}$ line-to-continuum ratio) for IRc2 is ~ 50 – higher than any other source in BN/KL (Gezari et al. 1998). Due to the correlation with source structure, the extinguishing grains are probably local to IRc2 itself. The dereddened flux densities in the mid-IR for IRc2 indicate a color temperature of ≈ 240 K and a total luminosity of $L = 1000 \pm 500 L_{\odot}$ (Gezari et al. 1998). At least part of the strong silicate absorption could be due to the hot core, which clearly overlaps some of the mid-IR emission (Figure 6).

The IRc2 sources also show significant polarization in the near-IR (Minchin et al. 1991; Dougados et al. 1993). The high-resolution L' polarimetry map by Dougados et al. (1993) clearly shows linear polarizations of $10 - 15\%$ for the IRc2 sources with polarization angles roughly perpendicular to the direction of source I. This naturally leads to the interpretation that some of near-IR emission from IRc2 is due to scattering of radiation from source I.

The wavelength dependent morphology of IRc2 (Fig. 2) displays two important characteristics:

1. the resolved structure of IRc2 at $12.5 \mu\text{m}$ becomes more unresolved at shorter wavelengths, culminating in the point-like nature of sources A – D at L' ; and
2. the $3.8 - 5.0 \mu\text{m}$ sources A – D generally appear at the periphery of the $12.5 \mu\text{m}$ emission.

How to interpret these characteristics, however, is not at all clear: the first characteristic suggests that these sources are embedded protostars (as indicated by the mid-IR color of IRc2); while the second is indicative of an externally heated clump of gas and dust (as suggested by the near-IR polarimetry results). In addition, IRc2 appears to be partially extinguished by a tongue of dense foreground material which is revealed by a small bay in the extended $12 \mu\text{m}$ emission at $(\Delta\alpha, \Delta\delta) = (5.25, -7.80)$, and coincides with a small protrusion in the NH_3 emission (Figure 6), so patchy extinction plays a strong role in the observed morphology as well.

If sources A – E were indeed embedded protostars, then the total IR luminosity for IRc2, $L = 1000 \pm 500 L_{\odot}$ indicates that their masses would likely be in the $3 - 8 M_{\odot}$ range. This would imply that, in the 500-AU-diameter region where the IRc2 cluster sources are located, the volume averaged density would be larger than 10^{10} cm^{-3} . This would represent a compression by at least a factor of ~ 50 in all three dimensions relative to the density of a typical star-forming cloud core, 10^5 cm^{-3} and the original cloud core would have to have been larger than the whole BN/KL region. Therefore, while it is probably not impossible to get a group of massive stars forming so close to each other (the challenge is avoiding the centrifugal barrier during the collapse), it seems far more likely that sources A – E are patches of reflecting dust rather than embedded protostars.

In addition, the near-IR polarization and wavelength-dependent morphology of IRc2 from 3.8 to $12.5 \mu\text{m}$ point strongly to external heating and illumination. Indeed, it seems very likely that IRc2 is illuminated and heated by radiation and outflow-driven shocks from source I—especially if the outflow is oriented along a NW–SE axis (Greenhill et al. 1998). Assuming that the luminosity of source I is a reasonable $L \sim 10^4 L_{\odot}$, corresponding to a $10 - 20 M_{\odot}$ star, IRc2 would have to intercept $\sim 10\%$ of its total energy to account for its luminosity. Given the apparent relative placement of the IRc2 components and source I, this appears to be a plausible number. It is possible, however, that both external and internal heating play a role in the emission from IRc2, as would be expected if a low-mass, dense protostellar cocoon were placed very near an energetic source. Such objects would be the evolutionary forebears of the “proplyds” seen near the Trapezium.

It is interesting to note that IRc2 A is clearly coincident with the shell H_2O masers NE of source I, especially at $5.0 \mu\text{m}$ (Figure 6). If the outflow from source I is instead oriented along a NE–SW axis, as suggested by Greenhill et al. (2003), then IRc2 A may be thermal emission from the cavity being excavated out of the hot core by source I. The rest of the IRc2 sources might be shadowed by I’s circumstellar disk and hence would be self-luminous and/or heated by source n and BN.

4.3. The OMC 1 Outflows

As discussed in Section 1, observational evidence from a variety of tracers indicates that there are (at least) two outflows emerging from OMC 1. Radio CO and near-IR H_2 line emission show a fast, poorly collimated bipolar outflow along a NW–SE axis. On arcminute scales, the H_2 fingers appear to be erupting roughly orthogonal to the NH_3 ridge (Figure 7). Closer in, the shocked regions are correlated, but not coincident, with clouds observed at $12\ \mu\text{m}$ (Figure 4), suggesting that the H_2 emission arises from the shocked surfaces of warm clouds. A plausible explanation is that the fingers represent high velocity ejecta moving relatively unimpeded into low density regions NW and SE of the core, whereas the masers represent strong shocks at the locations where the ejecta encounter some dense gas in the OMC 1 ridge.

Recent VLBA observations of the SiO masers have been interpreted as evidence that the disk around source I has a minor axis oriented towards $\text{PA} = 45^\circ$ (Greenhill et al. 2003), roughly 90° from the previous interpretation by Greenhill et al. (1998). If this is correct, then there is no obvious source for the high-velocity “explosive” outflow originating from the hot core and aligned NW–SE as traced by CO and H_2 emission. But there are several alternative possibilities: First, it is possible that the disk orientation has flipped by about 90° within the last 1,000 years since the production of the H_2 fingers. Obviously, this hypothesis invokes a set of rather peculiar circumstances. Such an orientation change may be induced by the close passage of another massive star, or the sudden accretion of material with radically different angular momentum orientation. Second, perhaps one (or both) of the sources, I and n, suffered a major eruption that was more or less isotropic. As this flow ran into the NE–SW oriented ridge of dense gas traced by NH_3 observations, it was blocked. Some of the ejecta may have been deflected along the density gradient to produce a SE–NW flow. The problem with this interpretation is that it does not explain why the source I disk did not cast a mechanical shadow along its plane. Finally, it is possible that the recent 7 mm observations of source I do not trace dust emission from a disk. Rather, this emission traces a dense thermal jet oriented SE–NW, exactly along the major axis of

the high velocity CO outflow and H_2 fingers. In this latter picture, the distribution of SiO masers within an arc second of source I do not trace the surface of a disk, but rather the shear layer formed where the jet interacts with a thick torus or cored-sphere of circumstellar material. While the geometry of this hypothesis is compelling, the observed velocities of the SiO masers and the CO and H_2 fingers do not match: the SiO masers are generally red-shifted to the NW of source I and blue-shifted to the SE while the CO and H_2 emission shows exactly the opposite velocity distribution.

We suggest the following scenario for the BN/KL region. Most of the H_2O and OH masers (but not the “shell masers” in the immediate vicinity of source I) are produced by a relatively steady bipolar outflow from source n (corresponding to the “ $18\ \text{km s}^{-1}$ ” flow, Genzel et al. 1981) which has cleared two cavities to the NE and SW. The H_2O maser motions suggest that this outflow has been active for at least 3000 years. The relationship between the explosive outflow associated with the H_2 fingers and oriented NW–SE and the outflow from source n is not clear, though both have probably contributed to the production of high velocity gas in the BN/KL region. These flows have similar dynamical ages and it is not clear which flow started first. If the explosive ejecta moved relatively unimpeded through the medium, then the flow from source n may have cleared a cavity before the explosive event traced by the H_2 fingers. The limited spatial extent of the “shell masers” suggests that source I may be younger than source n.

An interesting feature of the NE and SW outflow cavities is the apparent anti-correlation of OH and H_2O masers (Figure 5): the NE cavity is dominated by OH masers and the SW by H_2O masers. This discrepancy might be because of the photodissociation of H_2O in the NE cavity by strong UV radiation from source I, n, BN, or perhaps even $\theta^1\ \text{C Orionis}$. The SW cavity may be shielded from any UV flux from source I and BN (though not n) allowing H_2O to survive and form maser spots.

4.4. IR source “t”

The mid-IR and H_2 emission north of IR source “t” (SE of IRC2; Figure 4) trace a semi-circle of H_2 emission with a diameter of $\sim 3''$ ($1370\ \text{AU}$ at 450

pc). The $12.5\ \mu\text{m}$ emission south of IRC11 forms a foot-shaped ridge following the H_2 emission north of source t. In addition, the mid-IR sources IRC8 and 22 appear to continue the circular structure around source t to the south.

H_2 emission can arise in both shock-excited regions and gas heated to a few thousand K by UV radiation. The circular structure around source t is highly suggestive of a PDR expanding into a higher density cloud – which can be accommodated if source t is a hot star on the near side, and close to the surface, of the hot core. If this hypothesis is correct, then source t must also be a significant source of UV flux, though not necessarily in the Lyman continuum since H_2 is excited by soft-UV photons. Thus, source t may be a late B or early A star. As the PDR advances outward from source t, the radiation front illuminates over-dense regions which then emit in the mid-IR. We postulate that the local extinction is somewhat higher to the south of t, blocking $2\ \mu\text{m}$ H_2 emission from the southern part of the PDR, while allowing $12.5\ \mu\text{m}$ emission from IRC8 and 22 to pass. The interface of the PDR with the IRC11 “foot” seems to be viewed nearly edge-on.

5. Summary & Conclusions

In this paper we have presented the highest spatial resolution map at $12.5\ \mu\text{m}$ of the BN/KL region to date. Despite relatively poor flux calibration owing to variable atmospheric transmission we were able to detect 6 new sources and resolve new morphologies for existing sources leading to the following results:

- IRC2 is resolved into multiple sources, as observed at $\sim 4\ \mu\text{m}$ (Dougados et al. 1993). The point-like nature of sources A – D at $3.8\ \mu\text{m}$ coupled with the relatively high color temperature of IRC2 in the mid-IR, seems to suggest that these are self-luminous sources. Near-IR polarization maps, however, suggest that IRC2 is externally illuminated. Comparison of our $12.5\ \mu\text{m}$ map with previous datasets clearly show that the shorter wavelength sources all appear at the periphery of the $12.5\ \mu\text{m}$ emission. This lends some weight to the picture in which IRC2 is illuminated and heated by source I, but we cannot rule out the possibility that IRC2 is a small

group of nearby protostars.

- The elongated structure of near-IR source n at $12\ \mu\text{m}$, coupled with the geometry of the mid-IR and NH_3 emission, and the location of H_2O and OH maser spots, is highly suggestive of a disk with rotation axis along a NE–SW axis on the sky. Thus, source n may be responsible for the low-velocity $18\ \text{km s}^{-1}$ flow emerging from OMC 1.
- In addition, we have discovered an arc of emission associated with the BN object and some interesting morphology for IR source t, SE of IRC2. The BN SW arc is a curious feature that requires follow-up imaging and spectroscopy at other wavelengths to determine its true nature.

Owing to the extreme obscuration on the line of sight, our mid-IR observations are only sampling the most massive end of the IMF in BN/KL. The stellar density in the region is likely to be very high (as suggested by the source I–IRC2 group), perhaps even greater than the Trapezium cluster. This high stellar density may be due to environment or evolutionary state (or both): It is possible that the Trapezium Cluster also began with a much higher stellar density. Additional deep mid-IR observations, especially at 4 and $8\ \mu\text{m}$ accompanied by $20\ \mu\text{m}$ images to determine spectral energy distributions, are required to determine the full stellar content of this rich environment.

The authors would like to thank an anonymous referee whose comments improved this manuscript substantially. This research has been supported by a cooperative agreement through the Universities Space Research Association (USRA) under grant # 85502-02-02 to M. Morris and by NASA Astrobiology grant NCC2-1052 to the University of Colorado.

Data presented herein were obtained at the W.M. Keck Observatory, which is operated as a scientific partnership among the California Institute of Technology, the University of California and the National Aeronautics and Space Administration. The Observatory was made possible by the generous financial support of the W.M. Keck Foundation. The authors wish to recognize and acknowledge the very significant cultural role and reverence that the summit of Mauna Kea has always had within the indigenous Hawaiian community. We are most fortunate to have the opportunity to conduct observations from this mountain.

Some of the data presented in this paper was obtained from the Multimission Archive at the Space Telescope Science Institute (MAST, <http://archive.stsci.edu/>). STScI is operated by the Association of Universities for Research in Astronomy, Inc., under NASA contract NAS5-26555. Support for MAST for non-HST data is provided by the NASA Office of Space Science via grant NAG5-7584 and by other grants and contracts.

REFERENCES

- Allen, D. A. & Burton, M. G. 1993, *Nature*, 363, 54
- Becklin, E. E. & Neugebauer, G. 1967, *ApJ*, 147, 799
- Blake, G. A., Sutton, E. C., Masson, C. R., & Phillips, T. G. 1987, *ApJ*, 315, 621
- Brown, P. D., Charnley, S. B., & Millar, T. J. 1988, *MNRAS*, 231, 409
- Chelli, A., Perrier, C., & Lena, P. 1984, *ApJ*, 280, 163
- Chernin, L. M. & Wright, M. C. H. 1996, *ApJ*, 467, 676
- Doeleman, S. S., Lonsdale, C. J., & Pelkey, S. 1999, *ApJ*, 510, L55
- Doi, T., O'Dell, C. R., & Hartigan, P. 2002, *AJ*, 124, 445
- Dougados, C., Lena, P., Ridgway, S. T., Christou, J. C., & Probst, R. G. 1993, *ApJ*, 406, 112
- Downes, D., Genzel, R., Becklin, E. E., & Wynn-Williams, C. G. 1981, *ApJ*, 244, 869
- Gaume, R. A., Wilson, T. L., Vrba, F. J., Johnston, K. J., & Schmid-Burgk, J. 1998, *ApJ*, 493, 940
- Genzel, R., Reid, M. J., Moran, J. M., & Downes, D. 1981, *ApJ*, 244, 884
- Genzel, R. & Stutzki, J. 1989, *ARA&A*, 27, 41
- Gezari, D. Y., Backman, D. E., & Werner, M. W. 1998, *ApJ*, 509, 283
- Greenhill, L. J., Chandler, C. J., Reid, M. J., Diamond, P. J., & Moran, J. M. 2003, in *IAU Symposium*
- Greenhill, L. J., Gezari, D. Y., Danchi, W. C., Najita, J., Monnier, J. D., & Tuthill, P. G. 2004, accepted by *ApJ*
- Greenhill, L. J., Gwinn, C. R., Schwartz, C., Moran, J. M., & Diamond, P. J. 1998, *Nature*, 396, 650
- Johnston, K. J., Migenes, V., & Norris, R. P. 1989, *ApJ*, 341, 847
- Jones, B. & Puetter, R. C. 1993, in *Proc. SPIE Vol. 1946*, p. 610-621, *Infrared Detectors and Instrumentation*, Albert M. Fowler; Ed., 610-621
- Kaifu, N., et al. 2000, *PASJ*, 52, 1
- Kwan, J. & Scoville, N. 1976, *ApJ*, 210, L39
- Lee, J.-K. & Burton, M. G. 2000, *MNRAS*, 315, 11
- Lonsdale, C. J., Becklin, E. E., Lee, T. J., & Stewart, J. M. 1982, *AJ*, 87, 1819
- Menten, K. M. & Reid, M. J. 1995, *ApJ*, 445, L157
- Minchin, N. R., Hough, J. H., McCall, A., Burton, M. G., McCaughrean, M. J., Aspin, C., Bailey, J. A., Axon, D. J., & Sato, S. 1991, *MNRAS*, 248, 715
- Morris, M., Palmer, P., & Zuckerman, B. 1980, *ApJ*, 237, 1
- Rieke, G. H., Low, F. J., & Kleinmann, D. E. 1973, *ApJ*, 186, L7+
- Schultz, A. S. B., Colgan, S. W. J., Erickson, E. F., Kaufman, M. J., Hollenbach, D. J., O'dell, C. R., Young, E. T., & Chen, H. 1999, *ApJ*, 511, 282
- Stolovy, S. R., Burton, M. G., Erickson, E. F., Kaufman, M. J., Chrysostomou, A., Young, E. T., Colgan, S. W. J., Axon, D. J., Thompson, R. I., Rieke, M. J., & Schneider, G. 1998, *ApJ*, 492, L151+
- Wilson, T. L., Gaume, R. A., Gensheimer, P., & Johnston, K. J. 2000, *ApJ*, 538, 665

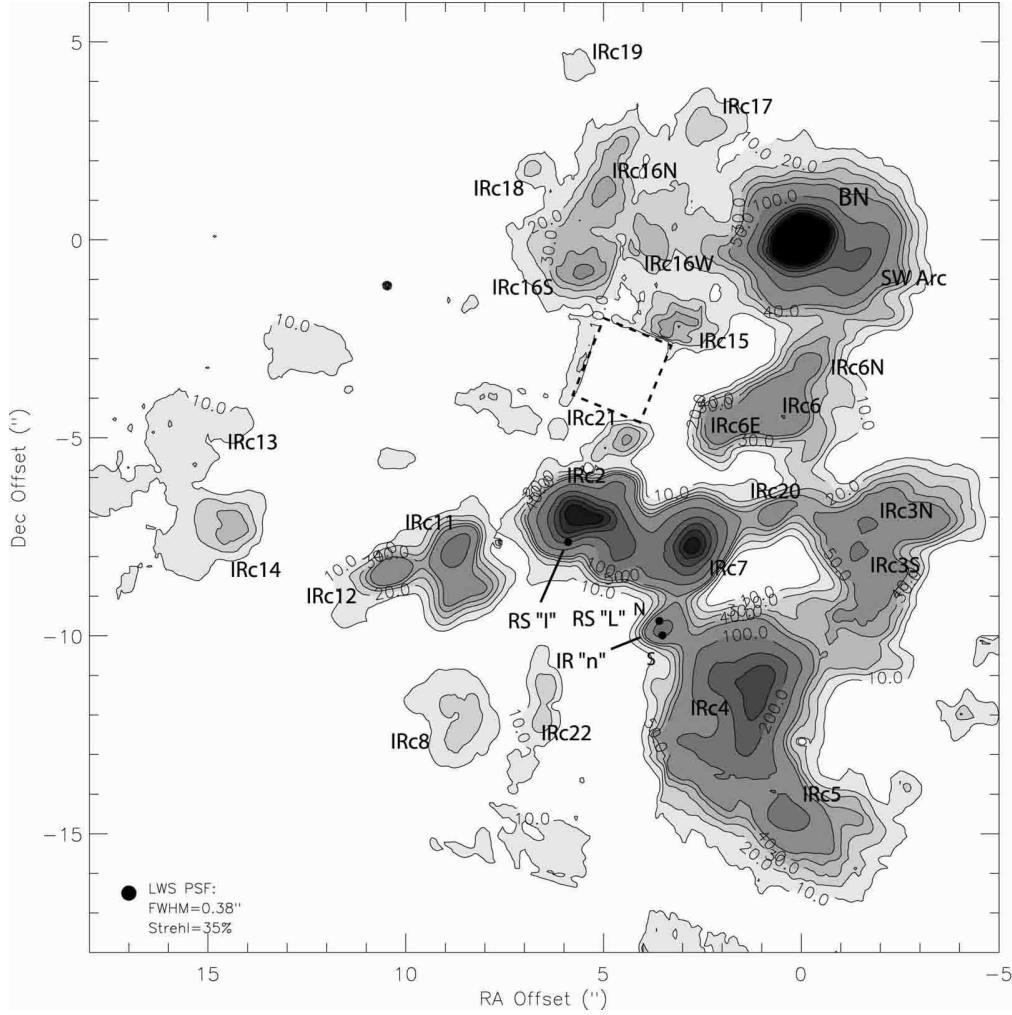


Fig. 1.— Filled contour map of the Keck/LWS 12.5 μm mosaic for BN/KL. Flux is mJy per $0.081 \times 0.081''$ pixel. Contours shown are for 10, 20, 30, 40, 50, 100, 200, 300, 400, 500, 600, and 6000 mJy; representative contours are marked in the figure. The dashed box shows the area not covered by our observations. Coordinates are centered on the BN object (RA = 05h35m14.117s, DEC = -05°22'22.90"[J2000]). See Table 1 for IR source identifications. Continuum radio sources (RS) "I" and "L" are also indicated (Menten & Reid 1995).

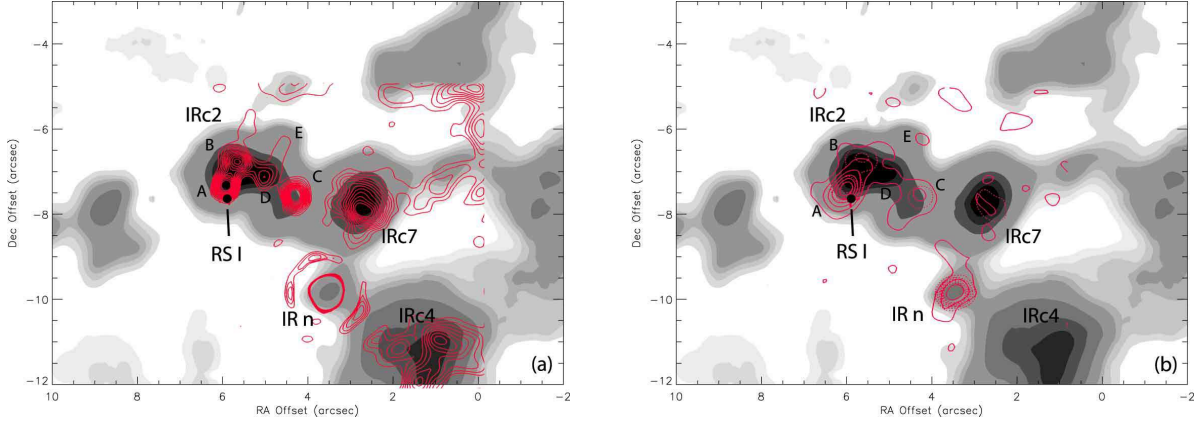


Fig. 2.— Filled contour map of the $12.5\mu\text{m}$ mosaic in the IRC2 region (grayscale, same contours as Fig. 1) overlaid with (a) L' emission and (b) 4.0 (dashed) and 5.0 (solid) μm emission (Dougados et al. 1993) in red contours. The spatial resolution of the $\sim 4\mu\text{m}$ data is $\text{FWHM} = 0.5''$. See Table 1 for IR source identifications.

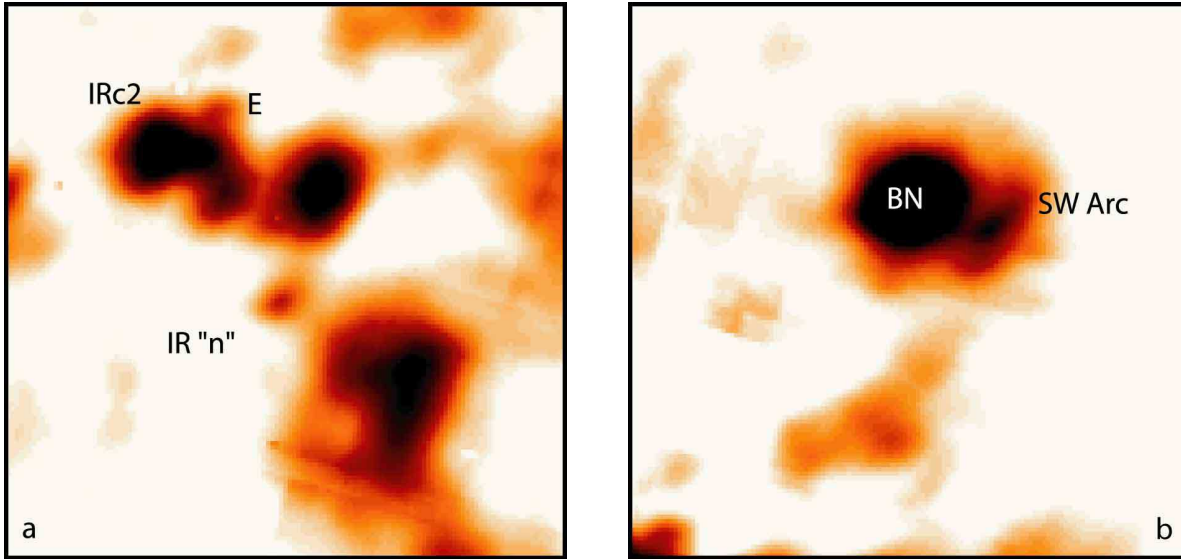


Fig. 3.— Detailed $12.5\mu\text{m}$ sub-images ($10'' \times 10''$) enhancing low level emission around near-IR source n (a) and the BN SW arc (b).

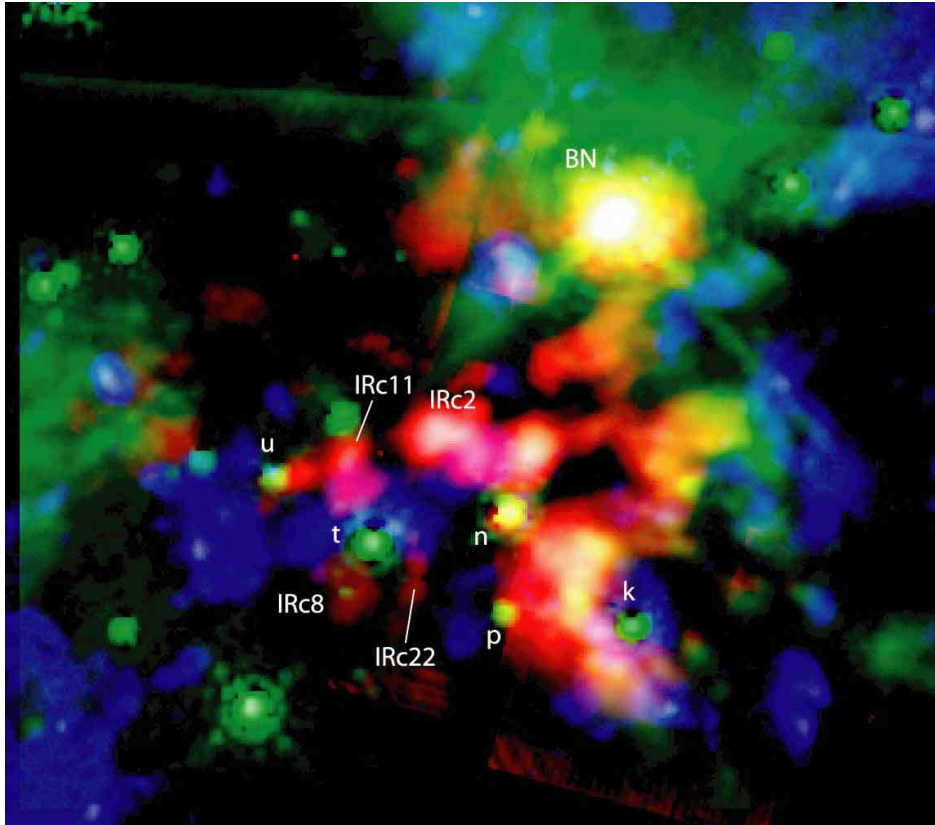


Fig. 4.— Three-color composite image of BNKL region ($31'' \times 27''$): Red = $12.5\mu\text{m}$ (this work); Green = NICMOS $2.15\mu\text{m}$ continuum; Blue = $2.12\mu\text{m}$ H_2 emission (NICMOS N212 – N215). A logarithmic stretch has been applied to each channel independently. To avoid confusion, stellar features in the H_2 channel (blue) have been masked out. The NICMOS data were obtained from the Multi-Mission Archive at Space Telescope and were first published by Schultz et al. (1999).

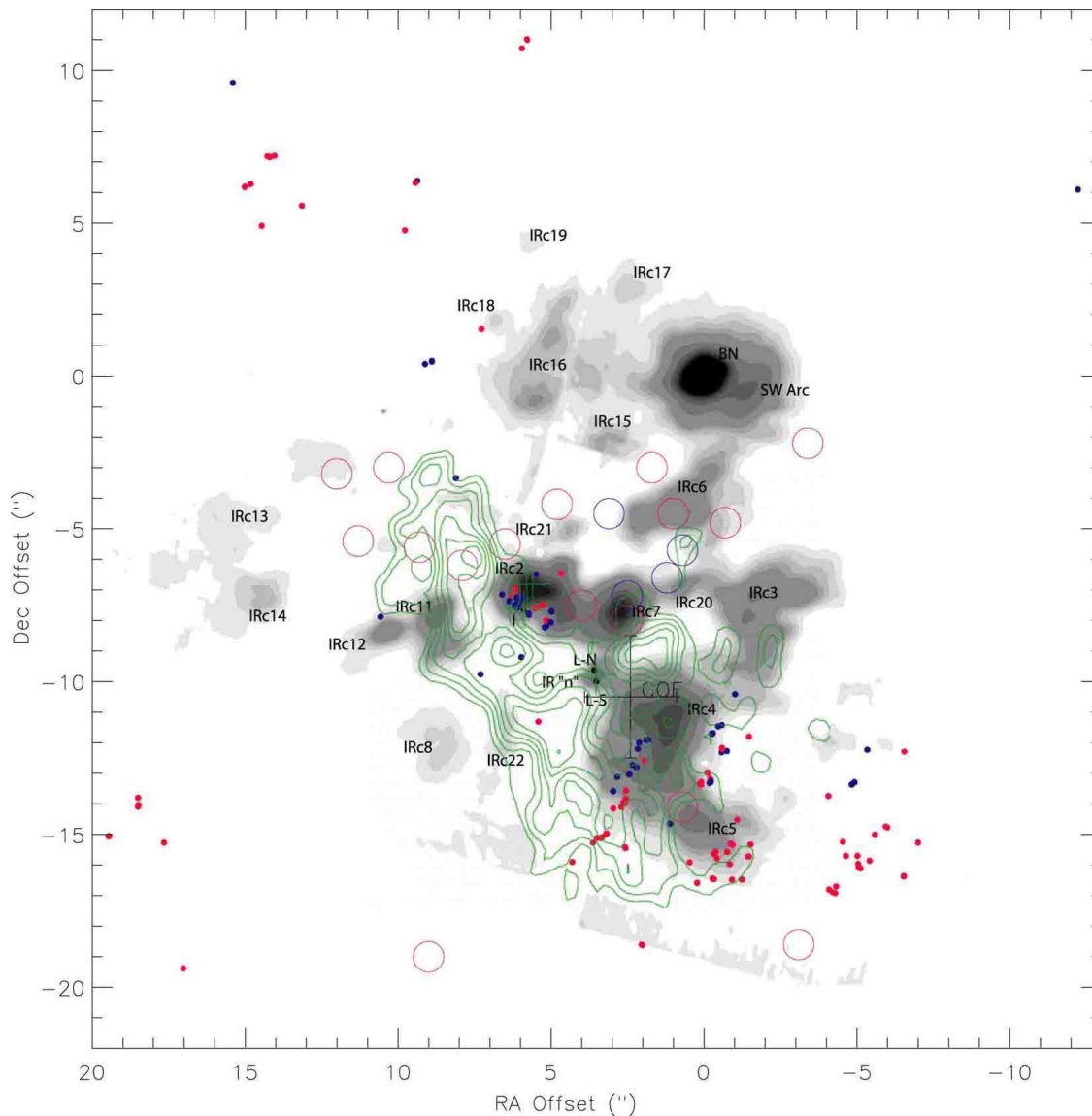


Fig. 5.— Filled contour map of the $12.5 \mu\text{m}$ mosaic (grayscale, same contour levels as Fig 1) overlaid with NH_3 emission at $V_{lsr} = 6.79 \text{ km s}^{-1}$ (green contours) tracing the Orion “hot core” (Wilson et al. 2000), H_2O masers (filled dots, Genzel et al. 1981; Gaume et al. 1998), and OH maser *clusters* (open circles, Johnston et al. 1989). Red and blue indicate Doppler shift for the maser(s) relative to $V_{lsr} = 5 \text{ km s}^{-1}$, the approximate velocity centroid of the hot core. The 18 km s^{-1} H_2O maser outflow center of expansion (COE) is remarkably close to IR source “n”. Notice the significant anti-correlation of NH_3 and $12 \mu\text{m}$ emission, suggesting that most of the mid-IR emission comes from at, or behind the hot core. The mid-IR emission and maser spots appear to trace bipolar cavities centered on source “n”. Offsets are relative to BN in arcseconds.

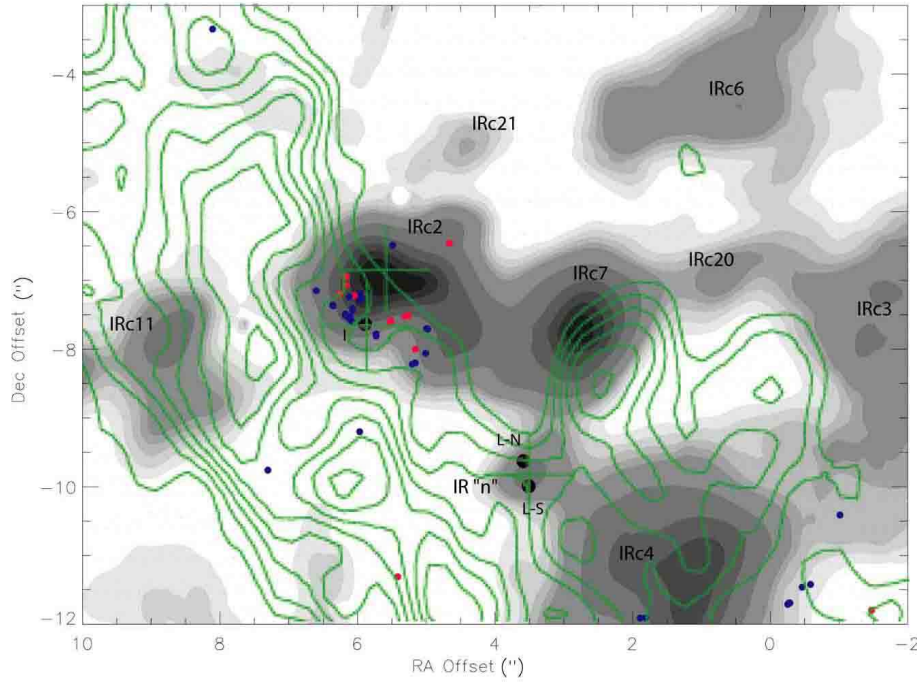


Fig. 6.— Filled contour map of the $12.5\mu\text{m}$ mosaic (grayscale, same contours as Fig. 1) overlaid with NH_3 emission at $v_{\text{lsr}} = 5.57 \text{ km s}^{-1}$ (green contours) tracing the Orion “hot core” (Wilson et al. 2000), H_2O masers (filled dots, Genzel et al. 1981; Gaume et al. 1998). Red and blue indicate Doppler shift for the maser(s) relative to $v_{\text{lsr}} = 5 \text{ km s}^{-1}$, the approximate velocity centroid of the hot core. The ammonia emission strongly suggests a cavity surrounding radio source I with a “thumb” of dense material occulting the southern part of IRc2. The “shell masers” surrounding source I may arise in shocked regions in the cavity wall. Offsets are relative to BN in arcseconds.

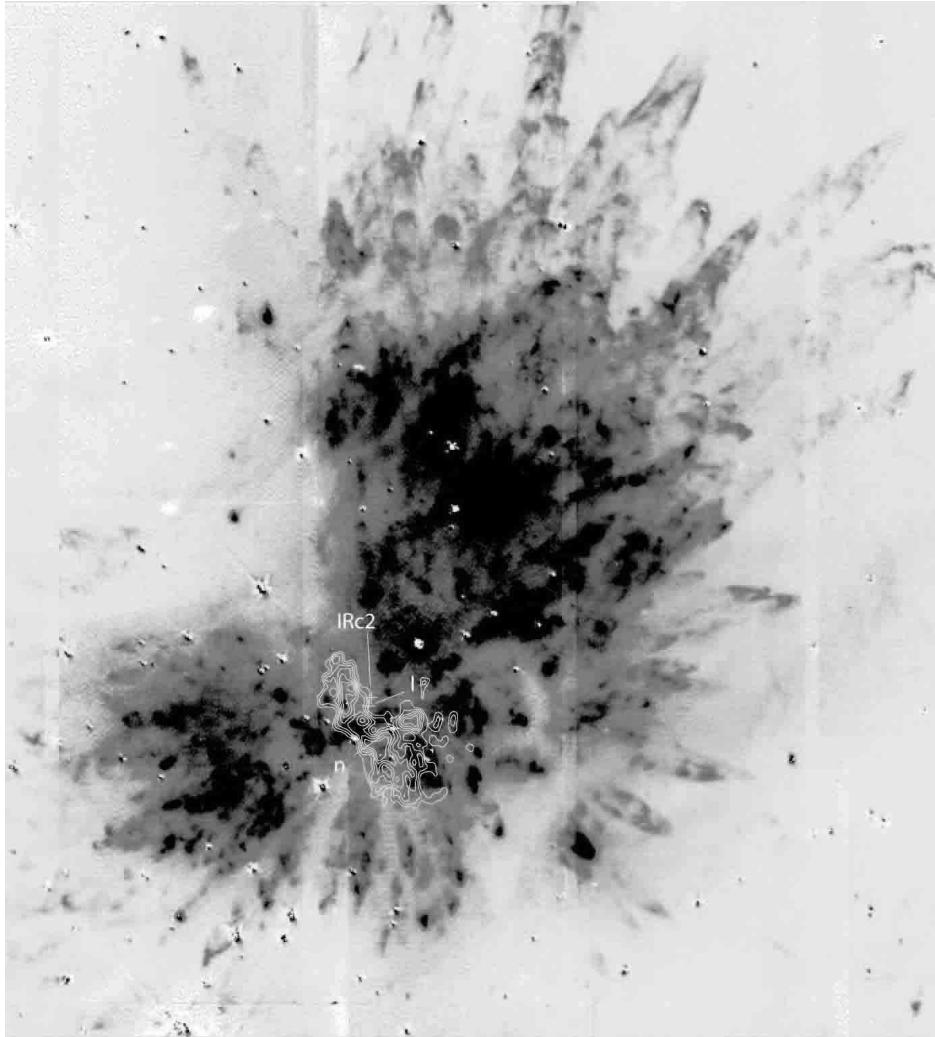


Fig. 7.— H_2 image of the OMC 1 region (Subaru Observatory) overlaid with NH_3 emission contours tracing the Orion hot core (Wilson et al. 2000). The image is roughly $2' \times 2'$ in size.

TABLE 1
MID-IR SOURCES IN BN/KL

Name	Offset ^a RA (″)	Offset ^a Dec. (″)	Positional Error (″)	Flux (Jy) ^b	Aperture Radius (″)	Notes	Refs.
BN	0.0	0.0	0.1	[600]	2.025		2,3
BN SWarc	-1.4	-0.6	0.1			Elongated along PA = 131°	1
IR n	3.5	-9.8	0.1	14.2	0.81		3,4
IRc2 A+B	5.7	-7.0	0.1	[120]	1.215	Single 12 μ m source between A & B	5
IRc2 C	4.6	-7.8	0.1				6
IRc2 D	5.0	-7.0	0.1				6
IRc2 E	4.7	-6.3	0.1				1,6
IRc3N	-1.6	-7.2	0.1				1
IRc3S	-1.4	-7.9	0.1				1
IRc4	1.1	-11.1	0.1			Position here is peak at NW vertex.	3,7
IRc5	0.5	-14.5	0.2	19	0.891		3,7
IRc6	0.4	-4.5	0.1			Central source	3,8
IRc6N	-0.2	-3.2	0.1				3
IRc6E	2.0	-4.8	0.1				1
IRc7	2.8	-7.8	0.1	108	1.215		3,8
IRc8	8.4	-12.2	0.2				3,8
IRc11	8.8	-7.9	0.2	18.7	0.81	Position and flux are for primary elliptical source	3
IRc12	10.3	-8.4	0.2	10.1	0.81		3
IRc13	14.5	-4.8	0.3			Diffuse, broken structure	3
IRc14	14.5	-7.2	0.3			Diffuse, broken structure	3
IRc15	3.1	-2.3	0.1			Position uncertain (edge)	3
IRc16N	4.9	1.3	0.2				1
IRc16S	5.5	-0.8	0.2				1
IRc16W	4.0	0.2	0.1				1
IRc17	2.5	2.8	0.1				3
IRc18	6.8	1.8	0.2	2.6	0.729		3
IRc19	5.7	4.2	0.2			Associated with NIR "q" ?	1,4
IRc20	0.7	-6.9	0.1	7.1	0.729		1
IRc21	4.4	-5.0	0.1	5.2	0.729		1
IRc22	6.4	-11.3	0.2			Faint N–S ridge	1

^aOffset from BN (RA = 05h35m14.117s, DEC = -05°22′22.90″, J2000)

^bTotal sky-subtracted flux measured in the aperture listed; the sky value was determined from an annulus just beyond the aperture. 2σ error for total flux is 10% – 27%, see text. Fluxes in brackets (BN and IRc2) are from Gezari et al. (1998) and were used for calibration.

References. — (1) This work; (2) Becklin & Neugebauer (1967); (3) Gezari et al. (1998); (4) Lonsdale et al. (1982); (5) Chelli et al. (1984); (6) Dougados et al. (1993); (7) Rieke et al. (1973); (8) Downes et al. (1981)